

Effect of Protonation and Deprotonation on Electron Transfer Mediated Decay and Interatomic Coulombic Decay

Ravi Kumar^{*†‡} Dr.Nayana Vaval^{§¶}

Abstract

Electronically excited atoms or molecules in an environment are often subject to interatomic/intermolecular Coulombic decay (ICD) and/or electron transfer mediated decay (ETMD) mechanisms. Various factors like, for instance, bond distance, number of surrounding atoms or molecules, and polarization effect affect these non-radiative decay mechanisms. In this paper, we have studied the effect of protonation and deprotonation on the ionization potential (IP), double ionization potential (DIP), and lifetimes (or decay width) of temporary bound states in these non-radiative decay processes. We have chosen LiH-NH₃ and LiH-H₂O as test systems. The equation of motion coupled cluster singles and doubles method augmented by a complex absorbing potential (CAP-EOM-CCSD) is used to calculate the energetic position of the decaying states and the system's decay rate. After ionization of the shallow core of Li and inner valence ionization of H₂O and NH₃, our analysis reveals that the deprotonation lowers the IP and DIP compared to the respective neutral systems. In contrast, protonation increases these quantities compared to the neutral systems. The lowering of the DIP due to deprotonation opens the decay channels, whereas protonation closes the relaxation channels for ICD/ETMD. Our study shows that the efficiency, i.e., the rate of ICD/ETMD, can be altered by protonation

*rs.kumar@ncl.res.in

†Academy of Scientific and Innovative Research, CSIR-Human Resource Development Center (CSIR-HRDC) Campus, Postal staff College Area, Ghaziabad, Uttar Pradesh, 201002, India

‡Electronic Structure Theory Group, Physical and Materials Chemistry Division, CSIR-National Chemical Laboratory, Pune, 411008, India

§np.vaval@ncl.res.in

¶Academy of Scientific and Innovative Research, CSIR-Human Resource Development Center (CSIR-HRDC) Campus, Postal staff College Area, Ghaziabad, Uttar Pradesh, 201002, India

‖Electronic Structure Theory Group, Physical and Materials Chemistry Division, CSIR-National Chemical Laboratory, Pune, 411008, India

and deprotonation. This is expected to have implications for chemical and biological systems.

Introduction

The knowledge on the importance of non-radiative processes like interatomic and intermolecular coulombic decay (ICD)^[1,2] and electron transfer mediated decay (ETMD)^[3-5] has substantially increased over the past two decades. ICD, first proposed by Cederbaum *et al.*,^[1,2] is a nonlocal and efficient decay mechanism that occurs at the femtosecond timescale. During this process, when an ionized/excited system relaxes non-radiatively in an environment, an outer valence electron fills the vacancy in the inner valence, resulting in a virtual photon emission which knocks out a valence electron from an adjacent atom or molecule. This situation leads to a Coulomb explosion due to the proximity of two positively charged species. The energy transfer happens quickly, i.e. in a few to a hundred femtoseconds. ICD was initially studied theoretically^[6-8] and experimentally^[9-14] in hydrogen-bonded,^[15] and weakly bound rare gas clusters.^[16,17] In ETMD, an electron is transferred from a neighboring atom to an initially ionized atom or molecule. The excess energy can knock out a second electron from the same donor atom/molecule in ETMD(2) process. While in ETMD(3), secondary electron ejection occurred from the second adjacent atom/molecule. Since ETMD involves the transfer of electrons from a neighboring species to an initially ionized species, it is usually slower than the ICD. See figure 1 for a better understanding of the difference between ICD and ETMD. The low energy electrons generated during ICD and ETMD have different kinetic energies. One can use this information to identify the specific local environment. Thus, the study of ICD and ETMD is essential to understand the decay of the ionized inner valence state in an environment. Recent studies^[18,19] show that various factors influence the ICD/ETMD process, like the number of surrounding atoms or molecules, bond distance, geometry, and the medium in which energy/electron transfer happens. The environment can change the lifetime of a temporary bound state (TBS) undergoing ICD / ETMD by stabilizing or destabilizing it. Thus, environmental effects/properties play a particularly relevant role. In this paper, we explore an important environmental effect: the protonation and deprotonation effect on ICD and ETMD. Specifically, we will study the impact of protonation and deprotonation on ionization potential (IP), Double ionization potential (DIP), and decay width (or the lifetime of TBS). Recently, the effect of protonation and deprotonation on IP and DIP in pure ammonia clusters^[20] has been studied. Still, the impact of protonation and deprotonation on the lifetime of TBS has not been studied. We are the first ones to learn it through this study.

Our aim is to understand the effect of protonation/deprotonation on the ICD/ETMD using alkali metal ions microsolvated in water and ammonia. Understanding this may help us control the relevant process in a chemical environment. This tells us how a change in surrounding and protonation/deprotonation

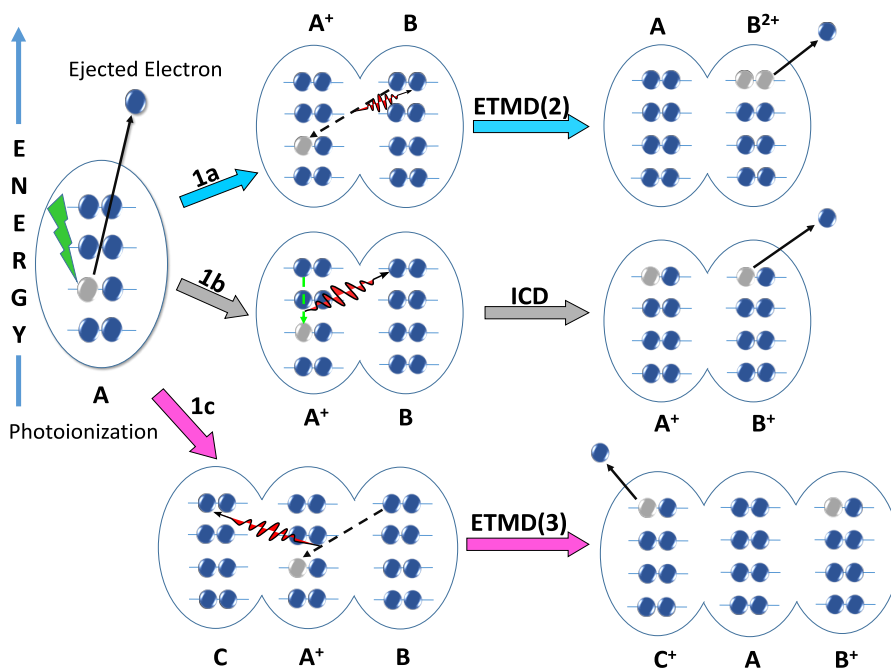


Figure 1: Visual representation of electronic decay processes. (1a.) In ETMD(2), an inner valence vacancy is filled by an outer valence electron of the neighboring atom B, and another valence electron is emitted from the same atom B leaving a final AB^{2+} state. (1b.) ICD, a valence electron from atom A, fills the vacancy, and the released energy is transferred to an outer valence electron of neighboring atom B. Thus, forming A^+B^+ as the final state. (1c.) ETMD(3) process in which the vacancy in atom A is filled by an outer valence electron of the neighboring atom B, and ejection of the second electron occurs from another adjacent atom C, leaving AB^+C^+ as the final state. The number 2 and 3 represents the number of atoms involved in the ETMD process.

affects the decay process and lifetime of the TBS. The first step towards this will be doing these calculations accurately for a metal ion-water system and its protonated/ deprotonated form with the coupled-cluster methods, which scale as N^6 . To get the decay width, we need to solve the CC equation thousands of times, which makes it computationally expensive. Thus, we wanted to study the smallest possible metal-related system. Therefore, we chose Lithium, although we know that the alkali metals Na^+ , K^+ , etc., are more relevant biologically. Also, as the first step towards this, gas-phase calculations are done. We may have to implement some approximate method for the actual interesting systems. We have discussed our finding and their possible reasons in the results and discussion section (next section), followed by the Conclusion. Last, we have discussed the Computational and Theoretical details of the Equation of motion

coupled cluster methods.

Results and Discussion

We will study the effect of protonation and deprotonation on the IP, DIP, and lifetime of O-2s, N-2s and Li-1s TBS in the gaseous state. We have chosen LiH-H₂O and LiH-NH₃ as test systems for our study. Protonation and deprotonation can occur either from LiH or H₂O/NH₃. Thus, LiH₂⁺-NH₃ and LiH-NH₄⁺ will be formed by the protonation of LiH-NH₃ and Li⁻-NH₃ and LiH-NH₂⁻ by deprotonation. Similarly, for the LiH-H₂O system, we have Li⁻-H₂O and LiH-OH⁻ as deprotonated and LiH₂⁺-H₂O only as a protonated system. LiH-H₃O⁺ is unstable, so we could not locate global minima for this structure. Understanding the impact of deprotonation and protonation on ICD and ETMD in microsolvated systems is a step toward helping us control these relevant and abundant processes in various chemical environments and may also be in biological systems. We will first study the effect of the protonation and deprotonation on IP and DIP for LiH-NH₃, LiH-H₂O, and their protonated and deprotonated form. Here we will see how different surroundings affect the IP and DIP of Li-1s. We will also analyze and compare the IP and DIP values within the neutral, protonated, and deprotonated forms. Later, we will examine the factors that affect TBS lifetime and whether it is possible to find a general trend in the lifetime of TBS on protonation and deprotonation. Moreover, we will also see how the surrounding affects the decay processes.

Effect of protonation and deprotonation on the IP and DIP.

Figure 2 and figure 3 show the inner and outer valence IP of the neutral, protonated, and deprotonated LiH-H₂O and LiH-NH₃ systems, respectively, and their lowest DIP values. We have written down a few observations from both figures (2nd and 3rd) and will provide possible explanations for them. First, we observe the decrease in IP and DIP values of the system with deprotonation and an increase after protonation. This is due to the decrease and increase in effective nuclear charge on deprotonation and protonation, respectively.

Second, from figure 3, if we compare the IP values of the two deprotonated systems of the LiH-NH₃, i.e., Li⁻-NH₃ and LiH-NH₂⁻. The IP values for all the states of Li⁻-NH₃ are higher than the corresponding LiH-NH₂⁻, except for the IP of HOMO. HOMO's IP of LiH-NH₂⁻ (3.06 eV) is more than HOMO's IP of Li⁻-NH₃ (0.33 eV), which is just opposite of the rest of the IP trend. A similar trend is observed between deprotonated systems of LiH-H₂O. Since the lowest IP values are too small for Li⁻-NH₃ and Li⁻-H₂O, we again calculated them using the delta CCSD(T) method (a higher level of theory) on the same basis set, i.e., aug-cc-pVTZ basis set.^[21] The new lowest ionization energy (IE) we have obtained for Li⁻-NH₃ and Li⁻-H₂O are 0.46 eV and 0.54 eV, respectively. It means our results are consistent. To check the stability of the system, we also checked the zero-point energy, which is 0.63 eV for Li⁻-H₂O and 1.00 eV for

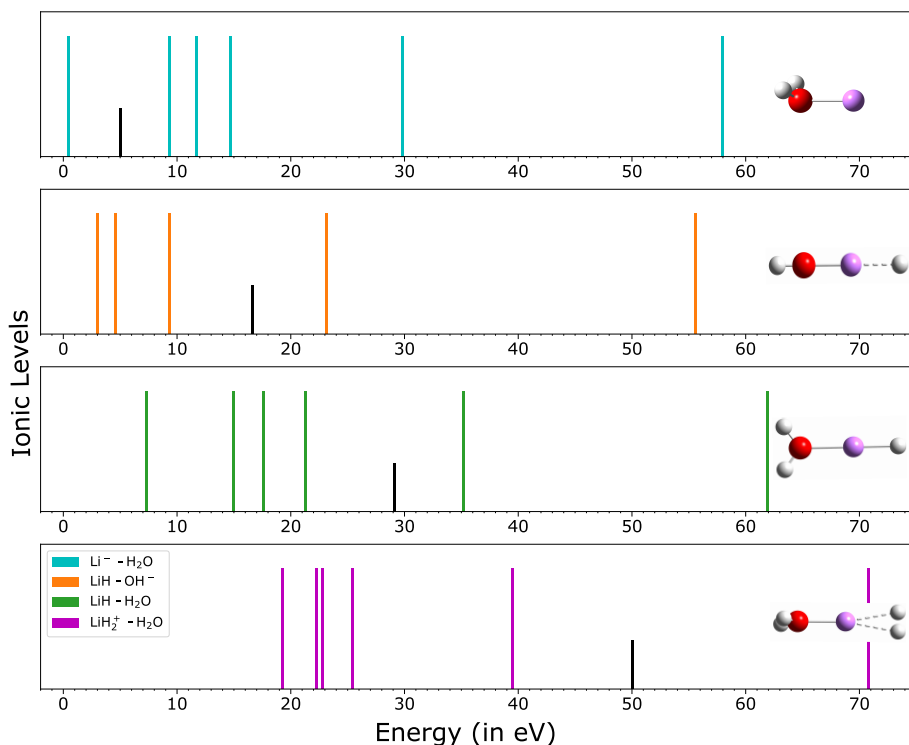


Figure 2: The IPs of neutral $\text{LiH-H}_2\text{O}$ and its deprotonated and protonated species. The smaller black line denotes the lowest DIP value. The structure of the respective system is shown on the right of each panel. Atom color code : Red: Oxygen, Pink: Lithium, and White: Hydrogen.

$\text{Li}^- \text{-NH}_3$. This means that both systems are unstable and can lose an electron vibrationally in their ground state, although the optimization had shown that these systems are stable. Thus, we will not study these systems further for decay width (or lifetime). The zero-point energy is calculated using the CCSD level of theory with the aug-cc-pVTZ basis set.^[21] Still, it is not clear why the lowest IP is so low. To understand that, we will discuss both systems' geometric and electronic structures before returning to the ionization spectra. Our primary focus will be the constitution of HOMO since HOMO does not fit the rest of the IP trend.

The HOMO of LiH-NH_3 and $\text{LiH-H}_2\text{O}$ is formed by lithium-2s and hydrogen-1s atomic orbitals. After deprotonation from LiH , HOMO is mainly $\text{Li}(2s)$ in $\text{Li}^- \text{-NH}_3$ and $\text{Li}^- \text{-H}_2\text{O}$. However, the HOMO of $\text{LiH-NH}_2^- / \text{LiH-OH}^-$ is similar to the corresponding neutral system. The LiH bond is ionic in nature, so electron density is shifted mainly towards the hydrogen in these systems. Figure 4(a,b and c) shows the location of HOMO ($\text{Li-}2s$), the lowest unoccupied molec-

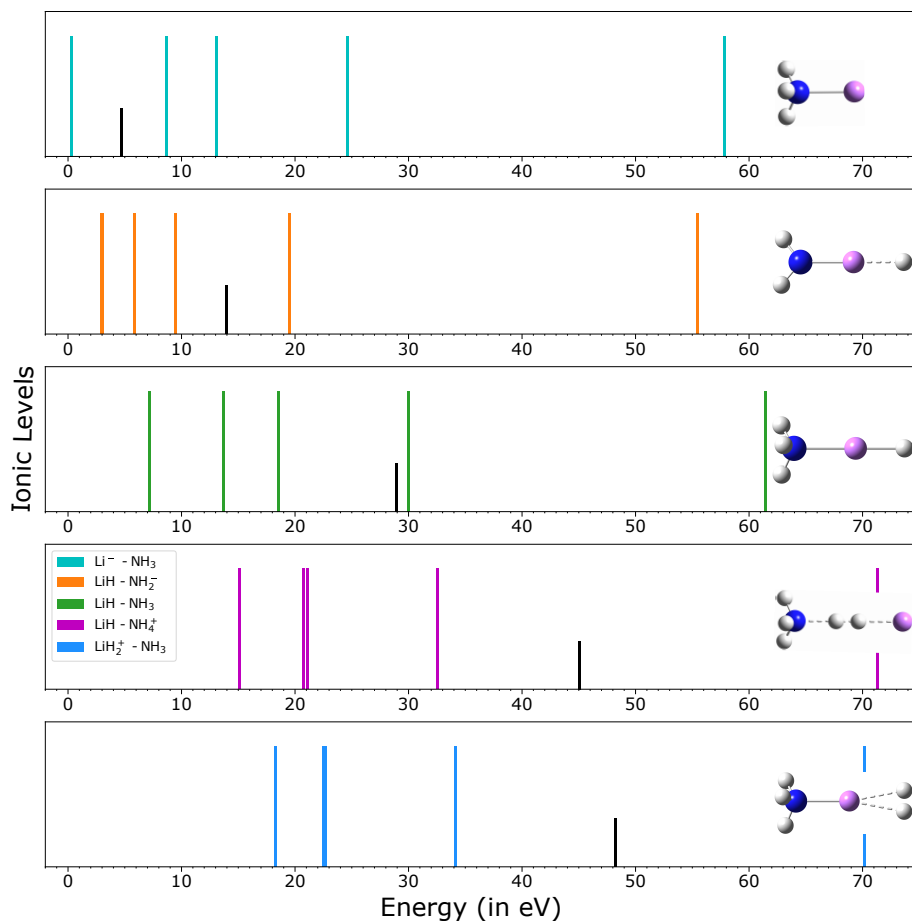


Figure 3: The IPs of deprotonated, protonated, and neutral LiH-NH₃. The smaller black line denotes the lowest DIP value. The structure of the respective system is shown on the right of each panel. Atom color code : Blue: Nitrogen, Pink: Lithium, and White: Hydrogen.

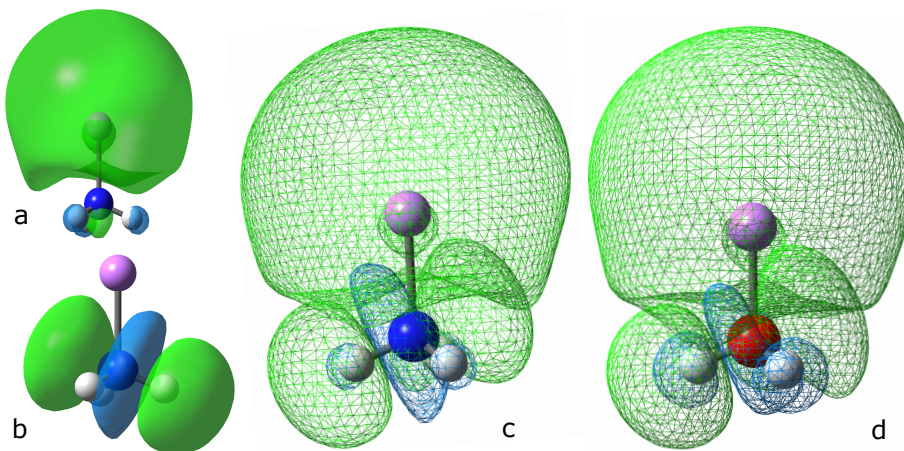


Figure 4: a and b are showing HOMO and LUMO in Li-NH₃. c and d are showing HOMO and LUMO are together in the one picture, demonstrating that they partially overlap in space for Li-NH₃ and Li-H₂O, respectively. Images are generated for 0.02 eÅ⁻³ isosurface value. Atom color code-: Blue: Nitrogen, Red: Oxygen, Pink: Lithium, and White: Hydrogen.

ular orbital (LUMO) (N-H antibonding), and both in one frame for Li⁻-NH₃. There is a partial overlapping of the HOMO and LUMO, which indicates the possibility of electron density transfer from HOMO to LUMO. Natural bond order (NBO) analysis proves this possibility, showing that the system stabilizes by $8.66 \times 3 = 25.98$ kcal/mol by delocalizing the electron density to 3 degenerate N-H antibonding orbitals from HOMO. Since the HOMO of Li(2s) is spherical, all three delocalizations can happen simultaneously. One more interaction stabilizing the system by 3.61 kcal/mol occurs between HOMO and Rydberg states (3s orbital) of N. Resulting in HOMO having negligible electron density. Hence, the IP of this HOMO is lowered dramatically to 0.33 eV in Li⁻-NH₃. The NBO analysis is done using the CCSD(T) level of theory and aug-cc-pVTZ basis set^[21] in the Gaussian09 software package^[22] and MOs in figure 4, are generated after NBO analysis. We do not observe similar interaction between HOMO and LUMO in the rest of the systems. We also calculated ionization energy using CCSD(T) level to confirm our finding.

A similar kind of partial overlapping in space (shown in figure 4d) and interaction between HOMO and LUMO is observed in Li⁻-H₂O. Here, the system stabilizes by $17.18 \times 2 = 34.36$ kcal/mol by delocalizing Li-2s electron density to 2 O-H antibonding orbitals, drastically lowering the IP of HOMO to 0.42 eV.

We have observed delocalization of electron density in Li⁻-NH₃ and Li⁻-H₂O. One can say why there is no delocalization in LiH-OH⁻ and LiH-NH₂⁻ since both are deprotonated systems too? An explanation for this is, first, oxygen/nitrogen in water/ammonia is more electronegative than lithium. Thus, the lone pair remains localized on oxygen/nitrogen. Second, in LiH-OH⁻ and

LiH-NH₂⁻, Li is bonded to the p_z-orbital of nitrogen and oxygen. After deprotonation, the electron density remains in x and y-direction (in p_x and p_y orbitals of N/O). P-orbitals are directional, unlike the s-orbital of Li-2s in Li⁻-NH₃ and Li⁻-H₂O, which is spherical. Thus, we do not see delocalization on deprotonation from ammonia/water in LiH-OH⁻ and LiH-NH₂⁻.

Third, we observe that the protonation of lithium hydride (leads to LiH₂⁺-NH₃) increases the IP more than the protonation of ammonia (leads to LiH-NH₄⁺). For example, the IP of HOMO is higher for LiH₂⁺-NH₃ (18.24 eV) than for LiH-NH₄⁺ (15.10 eV). The reason for it is the charge transfer. The location of a H⁺ ion is critical within the molecule because it can help promote and demote the charge transfer between Li and N. As discussed earlier, HOMO in LiH-NH₃ is more localized on hydrogen than lithium. An extra added H⁺ ion shifts the lithium's 2s electron density. Thus, almost all-electron density will be on H₂⁺ in LiH₂⁺-NH₃ and LiH-NH₄⁺, and lithium will be left with nearly nothing. But, this shortage of electron density on Li is overcome by the direct sharing of lone pair of ammonia in LiH₂⁺-NH₃, resulting in stabilizing the system. Since the added H⁺ ion is away from ammonia in LiH₂⁺-NH₃ (see figure 3 for geometry), this promotes the charge transfer even more. Such direct electron sharing is impossible from ammonia to lithium in LiH-NH₄⁺ since H₂⁺ is between lithium and nitrogen.

Fourth, we observe that the DIP value is the lowest (4.73 eV for Li⁻-NH₃) and highest (48.26 eV for LiH₂⁺-NH₃) when deprotonation and protonation occur from lithium hydride, respectively. That's because HOMO, which corresponds to the lowest DIP orbital, is a combination of lithium and hydrogen atomic orbitals. Thus, any change to these orbitals can lead to a considerable shift in DIP.

Until now, we have discussed the effect of protonation and deprotonation on IP and DIP values. We have observed that protonation increases the IP and DIP values resulting in closing of decay channels. For example, in LiH₂⁺-NH₃ and LiH-NH₄⁺, nitrogen 2s (inner valence) state stops showing the decay. Note that the IP and DIP of the protonated/deprotonated system tell us whether a system is temporarily bound or not. In other words, if decay is possible or not. However, it does not give any clue about the decay process (ICD or ETMD) and the actual value of the decay width. This means whether a lifetime of a decaying state will increase or decrease on protonation or deprotonation cannot be concluded based only on the IP and DIP values. To know that, now we will study how the protonation and deprotonation affect the decay width (in meV) and lifetime (in fs) of the TBS, along with the possible reasons.

Effect of protonation and deprotonation on the lifetime of Li-1s and O-2s/N-2s TBS in LiH-H₂O and LiH-NH₃.

Figure 1 shows the pictorial depiction of the ICD and ETMD processes for a general system AB. In ICD, the localization of the final two-hole states is on two different atoms, i.e., A⁺B⁺, while in ETMD(2), it's on one atom, i.e., AB²⁺ or A²⁺B. In ETMD(3), the two-hole localization is on two adjacent atoms.

Table 1: Energetic position of the decaying state and the decay width after Li-1s and O-2s ionization of LiH-H₂O along with its protonated and deprotonated systems.

System	Li-1s		O-2s	
	Energy(eV)	Width in meV (fs)	Energy (eV)	Width in meV (fs)
LiH-OH ⁻	55.56	64.27 (10.24)	23.10	16.6 (39.62)
LiH-H ₂ O	61.93	13.41 (49)	35.22	4.7 (139.6)
LiH ₂ ⁺ -H ₂ O	70.79	50.17 (13.17)	—	—

Thus, DIP eigenvalues and eigenvectors provide information about the possible decay channels. Table 1 and Table 2 report the energetic position of the decaying state and the decay width after Li-1s (core) and O-2s/N-2s ionization of LiH-H₂O and LiH-NH₃ along with their protonated and deprotonated systems. Next, we will discuss the possible reasons for the Li-2s and O-2s decay width (or lifetime) results by comparing the systems.

Comparing LiH-OH⁻ with LiH-H₂O, we observe a decrease in Li-1s TBS lifetime. The reason could follow as; we observed a reduction in O-Li bond length on moving from LiH-H₂O (1.924 Å) to LiH-OH⁻ (1.690 Å). Lithium has a more positive charge, and oxygen has a complete negative charge in LiH-OH⁻. Due to a decrease in the O-Li bond distance, the force of attraction increases, resulting in two lone pairs of oxygen shifting more toward Lithium (see fig. 5a and 5b). Electron density of LiH bond is mostly on hydrogen; thus, an incoming electron from oxygen might feel significantly less repulsion from Li-2s electrons. This makes the shift of electrons more favorable. This shift of lone pairs increases further when there is a vacancy formation on Li during the decay. Thus, we are getting a low lifetime for Li-1s TBS. Now we will study the decrease in Li-1s TBS lifetime in LiH-NH₂⁻. The reason is the occurrence of an extra lone pair on NH₂⁻ in LiH-NH₂⁻. This extra lone pair orbital shows partial overlapping with Li-1s orbital (see fig. 5c), making electron transfer even faster in LiH-NH₂⁻ than LiH-NH₃. Thus, we observe a decrease in the lifetime of Li-1s TBS in LiH-NH₂⁻.

We have observed a large change in the lifetime of O-2s TBS and slight drop in the N-2s TBS in LiH-OH⁻ and LiH-NH₂⁻ compared to their respective neutral systems. That's because for three reasons. First, LiH-OH⁻ has two lone pairs, which are perpendicular to the molecular plane, while LiH-NH₂⁻ has one. It means LiH-OH⁻ and LiH-NH₂⁻ each have one lone pair extra than their respective neutral systems. We know that lone pair electrons are influenced by one nucleus (atom specific), while bonded electron density is controlled by two attractive forces from two different nuclei. It means the O-2s or N-2s vacancy can occupy faster in deprotonated states than in respective neutral systems. Hence, we observed that the decay becomes faster, and the lifetime will reduce.

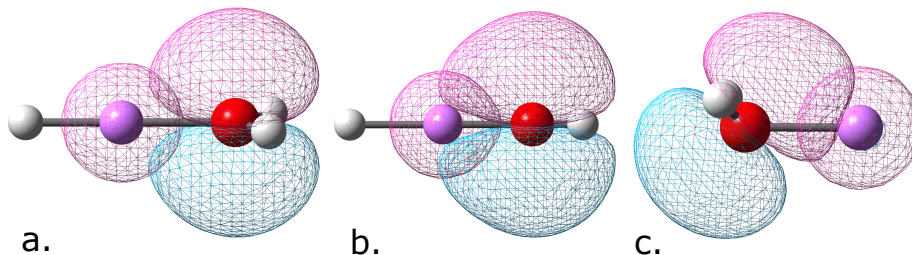


Figure 5: a, b, and c are showing the partially overlapping lone pair orbital and Li-1s orbital in space for $\text{LiH-H}_2\text{O}$, LiH-OH^- , and LiH-NH_2^- , respectively. From $\text{LiH-H}_2\text{O}$ to LiH-OH^- , the orbital's partial overlapping in space increases because the Li-O bond distance decreases and two opposite charges on adjacent atoms make this overlapping even stronger. Thus electron transfer becomes accessible, and Li-1s TBS decay faster. LiH-NH_3 and LiH-NH_2^- have a lone pair orbital along the molecular z-axis, but in LiH-NH_2^- one more lone pair orbital is present, which is perpendicular to the molecular plane and showing orbital's partial overlapping in space. It makes electron transfer a little faster from N to Li in LiH-NH_2^- than LiH-NH_3 . Images are generated for $0.02 \text{ e}\text{\AA}^{-3}$ isosurface value. Atom color code: Red: Oxygen, Pink: Lithium, Blue: Nitrogen, and White: Hydrogen.

Second, Oxygen is more electronegative than Nitrogen. Thus, attraction felt by electrons is higher in LiH-OH^- than LiH-NH_2^- , making decay faster. The third is the eigenvector analysis. We observe that N-2s have two possible decay channels in LiH-NH_2^- , while O-2s have four possible decay channels in LiH-OH^- . Based on eigenvector analysis, N-2s TBS decays by the ICD process only. In contrast, O-2s TBS decays by ETMD and ICD. All this is possible because of the huge change in geometry and symmetry of LiH-OH^- from $\text{LiH-H}_2\text{O}$. Here H-O-Li bond angle changes from 126.6° (in $\text{LiH-H}_2\text{O}$) to 180° (in LiH-OH^-), and symmetry changes to C_{2V} to $C_{\infty v}$. While in ammonia-related systems, the H-N-Li bond angle changes from 112.4° (in LiH-NH_3) to 127.9° (in LiH-NH_2^-), and symmetry changes from C_{3v} to C_{2v} . This change in geometry of the ammonia-related system is not profound compared to the geometry change of LiH-OH^- from $\text{LiH-H}_2\text{O}$.

The situation changes in $\text{LiH}_2^+-\text{H}_2\text{O}$ and $\text{LiH}_2^+-\text{NH}_3$ because the molecule can be seen as 3 separate units, i.e., $\text{H}_2\text{O}/\text{NH}_3$, Li^+ , and H_2 as 3 individual units. One can ask what difference it makes whether you see a molecule in 2 or 3 subunits. It makes the difference because the condition is correct for the ETMD(3) process (2 adjacent atom/molecule besides the TBS forming atom/molecule). Photoionization creates another positive charge on the lithium atom (Li-1s vacancy formation). An electron will come from the H_2 subunit to fill Li-1s vacancy, and the emitted virtual photon will eject another electron from NH_3 or H_2O . This is the ETMD(3) process. To explain an increase and decrease in Li-1s TBS, the directional nature of p-orbitals plays an important

Table 2: Energetic position of the decaying state and the decay width after Li-1s and N-2s ionization of Li-NH₃ along with its protonated and deprotonated systems.

System	Li-1s		N-2s	
	Energy(eV)	Width in meV (fs)	Energy (eV)	Width in meV (fs)
LiH-NH ₃	61.48	39.18 (16.79)	30.00	7.19 (91.48)
LiH ₂ ⁺ -NH ₃	70.17	10.39 (63.32)	—	—
	protonation and deprotonation on nitrogen			
LiH-NH ₂ ⁻	55.50	65.52 (10.45)	19.51	7.48 (87.90)
LiH-NH ₃	61.48	39.18 (16.79)	30.00	7.19 (91.48)
LiH-NH ₄ ⁺	71.01	144.06 (4.57)	—	—

role. In LiH₂⁺-H₂O, the orientation of the lone pair orbital of oxygen is perpendicular to the molecular plane, while in LiH₂⁺-NH₃, it's towards the Li-1s TBS. Due to this, charge transfer becomes easy in LiH₂⁺-NH₃, and we see Li-1s TBS is stabilized by the lone pairs of ammonia while there is no such stabilization from water in LiH₂⁺-H₂O. That's why we observe a decrease and increase in Li-1s TBS lifetime in LiH₂⁺-H₂O and LiH₂⁺-NH₃ than their neutral system, respectively. In LiH-NH₄⁺, there is no stabilization by the lone pair of ammonia since H₂ is in between Li and ammonia. Thus we observe a decrease in Li-1s TBS in LiH-NH₄⁺ than LiH-NH₃. As for O-2s decay in LiH₂⁺-H₂O, figure 2 shows that there is only one IP value (70.79 eV) higher than the lowest DIP value (50.03 eV) and that IP corresponds to Li-1s. That's the reason for getting the decay width only for Li-1s TBS and not for O-2s TBS. Not getting the O-2s peak in LiH-NH₄⁺ and LiH-NH₃ is similar to LiH₂⁺-H₂O.

Conclusions

The Li-1s TBS decays faster in LiH-NH₃ than LiH-H₂O because the orientation of the lone pair orbital of ammonia is toward Li, making electron transfer more quickly. Deprotonation increases the number of possible decay channels compared to the neutral system. Hence, we observe faster decay in the deprotonated system compared to the respective neutral system. On protonation, IP and DIP increase while deprotonation decreases IP and DIP. However, we do not observe such a general trend for the decay width/lifetime. In general, protonation/deprotonation of a molecule affects the structural stability, leading to pronounced changes in the geometry and charge distribution of the system. These two factors contribute to the difference in the decay width of the system. Unlike the IP/DIP values, we cannot say that protonation/deprotonation will increase/decrease decay width. For example, in water-related systems, geometry changes due to protonation/deprotonation dominating the decay widths.

However, in ammonia-related systems, we observe that charge transfer makes the system stable (i.e., $\text{LiH}_2^+-\text{NH}_3$), causing a significant difference in decay width. Based on eigenvector analysis Li-1s TBS decays via ICD and ETMD(2) in neutral and deprotonated systems. While Li-1s decays by ETMD(2 & 3) in $\text{LiH}_2^+-\text{NH}_3$ and $\text{LiH}_2^+-\text{H}_2\text{O}$. O-2s and N-2s TBS decay via ICD and ETMD(2) in the neutral system. But in deprotonated systems, N-2s decay via ICD (in $\text{LiH}-\text{NH}_2^-$) only while O-2s (in $\text{LiH}-\text{OH}^-$) decay via ICD and ETMD(2). In $\text{LiH}-\text{NH}_4^+$, all three decays are possible.

Theory and Computational Details

Before discussing the theory and methods behind the decay processes, we will discuss the computational details first. Geometries of all molecules were optimized in the Gaussian09 software package^[22] using B3LYP^[23-26] functional and 6-311++g(2d,p) basis set.^[27] The IPs of neutral, protonated, and deprotonated clusters are calculated using the equation of motion coupled-cluster singles and doubles (EOM-CCSD) method.^[28-31] The DIP values are computed using the diagonalization of the 2-hole block of EOM-CCSD. The decay position and width of the system are calculated using the EOM-CCSD method augmented by the complex absorbing potential (CAP).^[32-37] We have used the aug-cc-pVTZ basis set^[21] for CAP-EOM-CCSD calculations. See reference^[18] for details of the CAP-EOM-CCSD method for ICD, ETMD(2), and ETMD(3). We have run the CAP-EOM-CCSD calculations at different box sizes for both neutral systems. The dimension of optimum box size was found to be $C_x = C_y = C_z = 9$ a.u and δC in protonated, deprotonated, and neutral $\text{LiH}-\text{NH}_3$. $\delta C = R/2$ was added along the molecular axis. For protonated, deprotonated, and neutral $\text{LiH}-\text{H}_2\text{O}$ systems, box dimensions were $C_x = C_y = C_z = 11$ a.u and δC . Again, the $\delta C = R/2$ value was added along the molecular axis. Calculations of IP, DIP, and decay widths are done using homegrown codes. Now we will learn briefly about the CAP-EOM-CCSD method.

The target state, which is one hole state, is generated by the action of a linear operator $R(k)$ on the ground state wavefunction. The equation for the target state $|\Psi_k\rangle$ can be written as

$$|\Psi_k\rangle = R(k)|\Phi_{cc}\rangle \quad (1)$$

where $|\Phi_{cc}\rangle$ is the coupled-cluster wavefunction. It can be defined as

$$|\Phi_{cc}\rangle = e^T|\Phi_0\rangle \quad (2)$$

Where $|\Phi_0\rangle$ is the ground state Hartree-Fock wavefunction, $R(k)$ is an ionization operator, and T's ($T = T_1 + T_2$ for CCSD) are hole-particle excitation operators. T and R commute with each other. The linear operator R(k) within singles and doubles approximation is written as

$$R(k) = \sum_i r_i(k)i + \sum_{i,j,a} r_{ij}^a(k)a^\dagger ji \quad (3)$$

The similarity transformed Hamiltonian \overline{H}_N is formed as below.

$$\overline{H}_N = e^{-T} H_N e^T - \langle \Phi_0 | e^{-T} H_N e^T | \Phi_0 \rangle \quad (4)$$

The ionization potential values are obtained by diagonalizing the coupled-cluster similarity transformed Hamiltonian within $(N - 1)$ electron space. This similarity transformed Hamiltonian is formed within 1-hole and 2-hole one particle space.

$$\overline{H}_N R(k) | \Phi_0 \rangle = \omega_k R(k) | \Phi_0 \rangle \quad (5)$$

Where ω_k is the difference between the N and (N-1) electronic state, which is the IP of the k^{th} state.

The position and lifetime of the decaying state are obtained by augmenting the EOM-CCSD by complex absorbing potential (CAP). CAP approach adds a one-particle potential to the physical Hamiltonian $-i\eta W$. This makes the original Hamiltonian complex and non-hermitian $H(\eta) = H - i\eta W$. Where W is the real potential and η is the strength of CAP. The complex eigenvalues of the non-hermitian Hamiltonian give us the system's position and half decay width. In CAP-EOM-CCSD, we get the total decay width, i.e., the contribution from all possible decay channels. We do not get the decay width for the individual decay process.

We solve the $H(\eta) = H - i\eta W$ equation for various values of η to get the complex energies that are η dependent. Real part vs. imaginary part of energy plotted in energy plot which provides η trajectory. The stationary point on the trajectory provides the stabilization point.

Acknowledgment

RK acknowledges financial support from Council of scientific and Industrial Research. Authors acknowledge the computational facility at the CSIR-National Chemical Laboratory and IISER-Pune. Authors acknowledge Prof. L. S. Cederbaum for critical reading of the manuscript and the valuable suggestions.

Keywords

Ab-initio-calculations, Charge Transfer, Electron Mtransfer Mediated Decay, Ionization potential, Lithium ion.

TOC

Effect of protonation and deprotonation on ICD and ETMD (see picture 6) processes.

References

- [1] L. S. Cederbaum, J. Zobeley, F. Tarantelli, *Phys. Rev. Lett.* **1997**, *79*, 4778–4781.
- [2] R. Santra, L. S. Cederbaum, *Phys. Rep.* **2002**, *368*, 1–117.
- [3] J. Zobeley, R. Santra, L. S. Cederbaum, *J. Chem. Phys.* **2001**, *115*, 5076–5088.
- [4] I. B. Müller, L. S. Cederbaum, *J. Chem. Phys.* **2005**, *122*, 094305.
- [5] V. Stumpf, K. Gokhberg, L. S. Cederbaum, *Nat. Chem.* **2016**, *8*, 237–241.
- [6] S. Scheit, V. Averbukh, H. Meyer, N. Moiseyev, R. Santra, T. Sommerfeld, J. Zobeley, L. S. Cederbaum, *J. Chem. Phys.* **2004**, *121*, 8393–8398.
- [7] N. Vaval, L. S. Cederbaum, *J. Chem. Phys.* **2007**, *126*, 164110.
- [8] M. Ehara, T. Sommerfeld, *Chem. Phys. Lett.* **2012**, *537*, 107–112.
- [9] T. Jahnke, *J. Phys. B: At. Mol. Opt. Phys.* **2015**, *48*, 082001.
- [10] S. Marburger, O. Kugeler, U. Hergenhahn, T. Möller, *Phys. Rev. Lett.* **2003**, *90*, 203401.
- [11] T. Jahnke, A. Czasch, M. S. Schöffler, S. Schössler, A. Knapp, M. Käsz, J. Titze, C. Wimmer, K. Kreidi, R. E. Grisenti, A. Staudte, O. Jagutzki, U. Hergenhahn, H. Schmidt-Böcking, R. Dörner, *Phys. Rev. Lett.* **2004**, *93*, 163401.
- [12] I. Unger, R. Seidel, S. Thürmer, M. N. Pohl, E. F. Aziz, L. S. Cederbaum, E. Muchová, P. Slavíček, B. Winter, N. V. Kryzhevoi, *Nat. Chem* **2017**, *9*, 708–714.
- [13] M. N. Pohl, C. Richter, E. Lugovoy, R. Seidel, P. Slavíček, E. F. Aziz, B. Abel, B. Winter, U. Hergenhahn, *J. Phys. Chem. B* **2017**, *121*, 7709–7714, pMID: 28696722.
- [14] P. Zhang, C. Perry, T. T. Luu, D. Matselyukh, H. J. Wörner, *Phys. Rev. Lett.* **2022**, *128*, 133001.
- [15] S. D. Stoychev, A. I. Kuleff, L. S. Cederbaum, *J. Chem. Phys.* **2010**, *133*, 154307.

- [16] R. Santra, J. Zobeley, L. S. Cederbaum, N. Moiseyev, *Phys. Rev. Lett.* **2000**, *85*, 4490–4493.
- [17] N. Sisourat, H. Sann, N. V. Kryzhevoi, P. Kolorenč, T. Havermeier, F. Sturm, T. Jahnke, H. K. Kim, R. Dörner, L. S. Cederbaum, *Phys. Rev. Lett.* **2010**, *105*, 173401.
- [18] R. Kumar, A. Ghosh, N. Vaval, *J. Chem. Theory Comput.* **2022**, *18*, 807–816, pMID: 35019266.
- [19] T. Jahnke, U. Hergenbahn, B. Winter, R. Dörner, U. Fröhling, P. V. Demekhin, K. Gokhberg, L. S. Cederbaum, A. Ehresmann, A. Knie, A. Dreuw, *Chem. Rev.* **2020**, *120*, 11295–11369, pMID: 33035051.
- [20] N. V. Kryzhevoi, L. S. Cederbaum, *Angew. Chem. Int. Ed.* **2011**, *50*, 1306–1309.
- [21] R. A. Kendall, T. H. Dunning, R. J. Harrison, *J. Chem. Phys.* **1992**, *96*, 6796–6806.
- [22] M. J. Frisch, G. W. Trucks, H. B. Schlegel, G. E. Scuseria, M. A. Robb, J. R. Cheeseman, G. Scalmani, V. Barone, B. Mennucci, G. A. Petersson, H. Nakatsuji, M. Caricato, X. Li, H. P. Hratchian, A. F. Izmaylov, J. Bloino, G. Zheng, J. L. Sonnenberg, M. Hada, M. Ehara, K. Toyota, R. Fukuda, J. Hasegawa, M. Ishida, T. Nakajima, Y. Honda, O. Kitao, H. Nakai, T. Vreven, J. Montgomery, J. A., J. E. Peralta, F. Ogliaro, M. Bearpark, J. J. Heyd, E. Brothers, K. N. Kudin, V. N. Staroverov, R. Kobayashi, J. Normand, K. Raghavachari, A. Rendell, J. C. Burant, S. S. Iyengar, J. Tomasi, M. Cossi, N. Rega, J. M. Millam, M. Klene, J. E. Knox, J. B. Cross, V. Bakken, C. Adamo, J. Jaramillo, R. Gomperts, R. E. Stratmann, O. Yazyev, A. J. Austin, R. Cammi, C. Pomelli, J. W. Ochterski, R. L. Martin, K. Morokuma, V. G. Zakrzewski, G. A. Voth, P. Salvador, J. J. Dannenberg, S. Dapprich, A. D. Daniels, O. Farkas, J. B. Foresman, J. V. Ortiz, J. Cioslowski, D. J. Fox, Gaussian-09, Gaussian Inc., Wallingford CT, **2009**.
- [23] P. J. Stephens, F. J. Devlin, C. F. Chabalowski, M. J. Frisch, *J. Phys. Chem.* **1994**, *98*, 11623–11627.
- [24] A. D. Becke, *J. Chem. Phys.* **1993**, *98*, 5648–5652.
- [25] C. Lee, W. Yang, R. G. Parr, *Phys. Rev. B* **1988**, *37*, 785–789.
- [26] S. H. Vosko, L. Wilk, M. Nusair, *Can. J. Phys.* **1980**, *58*, 1200–1211.
- [27] R. Krishnan, J. S. Binkley, R. Seeger, J. A. Pople, *J. Chem. Phys.* **1980**, *72*, 650–654.
- [28] R. J. Bartlett, M. Musiał, *Rev. Mod. Phys.* **2007**, *79*, 291–352.

- [29] D. I. Lyakh, M. Musiał, V. F. Lotrich, R. J. Bartlett, *Chem. Rev.* **2012**, *112*, 182–243.
- [30] M. Nooijen, R. J. Bartlett, *J. Chem. Phys.* **1995**, *102*, 3629–3647.
- [31] J. F. Stanton, R. J. Bartlett, *J. Chem. Phys.* **1993**, *98*, 7029–7039.
- [32] T. Sommerfeld, U. V. Riss, H. D. Meyer, L. S. Cederbaum, B. Engels, H. U. Suter, *J. Phys. B: At. Mol. Opt. Phys.* **1998**, *31*, 4107–4122.
- [33] G. Jolicard, E. J. Austin, *Chem. Phys. Lett.* **1985**, *121*, 106–110.
- [34] U. V. Riss, H. D. Meyer, *J. Phys. B: At. Mol. Opt. Phys.* **1993**, *26*, 4503–4535.
- [35] J. Muga, J. Palao, B. Navarro, I. Egusquiza, *Phys. Rep.* **2004**, *395*, 357–426.
- [36] N. Moiseyev, *J. Phys. B: At. Mol. Opt. Phys.* **1998**, *31*, 1431–1441.
- [37] U. V. Riss, H. D. Meyer, *J. Phys. B: At. Mol. Opt. Phys.* **1998**, *31*, 2279–2304.

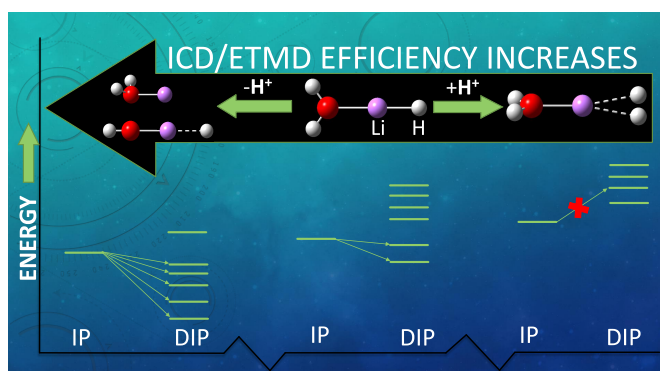


Figure 6: TOC